

Surface Engineering of Graphene through Heterobifunctional Supramolecular-Covalent Scaffolds for Rapid COVID-19 Biomarker Detection

Esteban Piccinini,^{*,§} Juan A. Allegretto,[§] Juliana Scotto, Agustín L. Cantillo, Gonzalo E. Fenoy, Waldemar A. Marmisollé, and Omar Azzaroni^{*}



Cite This: *ACS Appl. Mater. Interfaces* 2021, 13, 43696–43707



Read Online

ACCESS |



Metrics & More



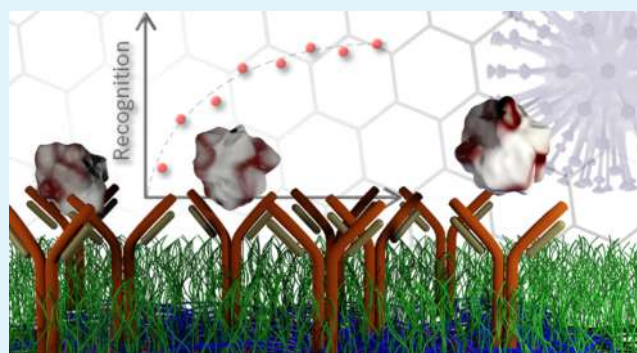
Article Recommendations



Supporting Information

ABSTRACT: Graphene is a two-dimensional semiconducting material whose application for diagnostics has been a real game-changer in terms of sensitivity and response time, variables of paramount importance to stop the COVID-19 spreading. Nevertheless, strategies for the modification of docking recognition and antifouling elements to obtain covalent-like stability without the disruption of the graphene band structure are still needed. In this work, we conducted surface engineering of graphene through heterofunctional supramolecular-covalent scaffolds based on vinylsulfonated-polyamines (PA-VS). In these scaffolds, one side binds graphene through multivalent π - π interactions with pyrene groups, and the other side presents vinylsulfonated pending groups that can be used for covalent binding. The construction of PA-VS scaffolds was demonstrated by spectroscopic ellipsometry, Raman spectroscopy, and contact angle measurements. The covalent binding of $-SH$, $-NH_2$, or $-OH$ groups was confirmed, and it evidenced great chemical versatility. After field-effect studies, we found that the PA-VS-based scaffolds do not disrupt the semiconducting properties of graphene. Moreover, the scaffolds were covalently modified with poly(ethylene glycol) (PEG), which improved the resistance to nonspecific proteins by almost 7-fold compared to the widely used PEG-monopyrene approach. The attachment of recognition elements to PA-VS was optimized for concanavalin A (ConA), a model lectin with a high affinity to glycans. Lastly, the platform was implemented for the rapid, sensitive, and regenerable recognition of SARS-CoV-2 spike protein and human ferritin in lab-made samples. Those two are the target molecules of major importance for the rapid detection and monitoring of COVID-19-positive patients. For that purpose, monoclonal antibodies (mAbs) were bound to the scaffolds, resulting in a surface coverage of $436 \pm 30 \text{ ng/cm}^2$. K_D affinity constants of 48.4 and 2.54 nM were obtained by surface plasmon resonance (SPR) spectroscopy for SARS-CoV-2 spike protein and human ferritin binding on these supramolecular scaffolds, respectively.

KEYWORDS: heterofunctional scaffold, graphene, supramolecular, antibody, COVID-19, SARS-CoV-2 spike protein



1. INTRODUCTION

Two-dimensional (2D) semiconducting materials such as graphene, hexagonal boron nitride (h-BN), and black phosphorus have attracted increasing interest during the past years due to their outstanding physicochemical, optical, and electronic properties.^{1–3} The use of these materials for diagnostic applications has helped overcome the current boundaries of sensitivity, response time, and sample processing.^{4,5} Due to its high conductivity, large specific area, and excellent chemical stability, graphene, a sheet of hexagonally arranged carbon atoms, is one of the most attractive 2D materials for the fabrication of biosensing devices.^{5–7} Its optical and electronic properties can be exploited in a broad variety of techniques; for instance, field-effect transistors (FET), photoelectrochemistry, fluorescence, and surface-

enhanced Raman scattering (SERS), in the development of sensing platforms. In particular, those biosensing platforms based on high-affinity complexes (e.g., antibody–antigen,⁸ CRISPR/Cas-target RNA,⁹ among others) show the greatest potential for the construction of ultrasensitive and ultrafast diagnostic devices. Moreover, rapid diagnostic tests (RDT) help to control the SARS-CoV-2 pandemic by the detection of COVID-19-infected people and monitoring of hospitalized

Received: June 28, 2021

Accepted: August 18, 2021

Published: September 2, 2021



(a) Non-covalent modification with PBSE:

(b) PA covalent modification of PBSE:

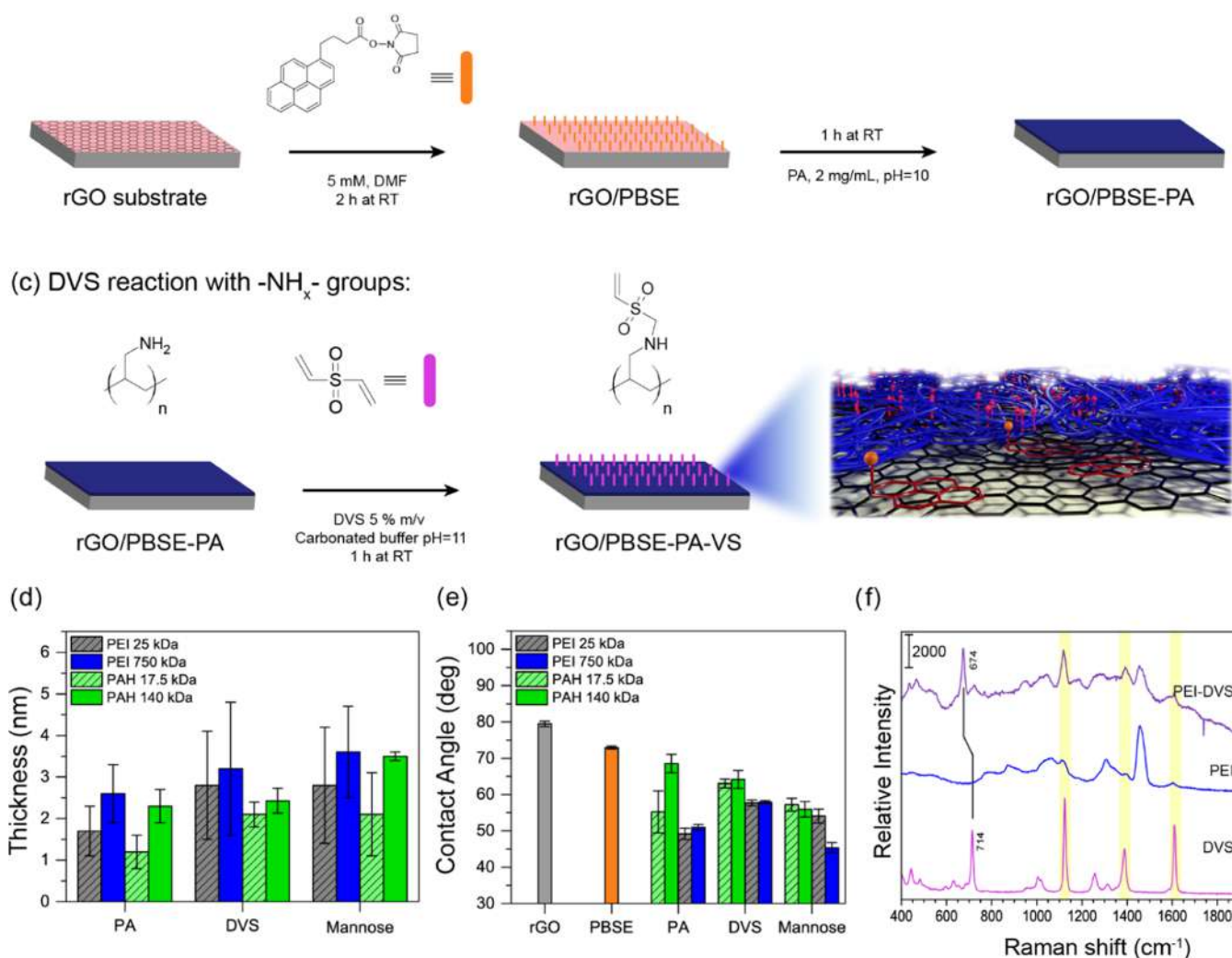


Figure 1. (a–c) Schematic representation of the functionalization steps for obtaining PA-VS surfaces. (d) Thickness and (e) contact angle evolution after different functionalization steps: PA anchoring on rGO/PBSE surfaces; changes after DVS functionalization (DVS); mannoseylation (Mannose). Error bars represent the 95% confidence interval. (f) Raman spectra of DVS, PEI (750 kDa), and the product of the reaction between them in aqueous solution (PEI-DVS).

patients.^{8,10–12} In this regard, certain common requirements are needed for reliable and high-performance-affinity biosensors based on 2D materials: (i) the anchoring of the recognition element to the 2D nanomaterial must preserve its affinity to the target entity; (ii) antifouling elements for avoiding nonspecific response from the biological sample must be incorporated; (iii) the modification methods should not cause the degradation of the inherent physicochemical properties of the transducing 2D nanomaterial; (iv) the biointerfaces must show good stability in the presence of surfactants that are typically used in extraction media for the preparation of samples; (v) the biointerface must be able to be regenerated to reuse the device. While many covalent and supramolecular approaches were reported to fulfil those requisites,¹³ there are still some challenges to surpass.

For instance, the direct covalent attachment to 2D semiconducting materials could induce lattice defects that hinder charge transport and, thus, impair signal transduction.^{14,15} This is the case of graphene covalent functionalization, which is accomplished using oxidized defects, such as

carboxyl or hydroxyl groups.¹⁶ As an attractive alternative, a heterobifunctional supramolecular architecture can be used. In this regard, a widely employed approach involves the immobilization of monopyrenes with reactive pendant groups (e.g., $-\text{COOH}$, $-\text{NH}_2$, $-\text{NHS}$) on graphene.¹⁷ Since monopyrenes attach to graphene by π - π interaction, the disruption of the aromatic chemical structure is avoided.¹⁶ However, and even when monopyrene linkers were reported to efficiently anchor some biomolecules,^{8,18,19} they are susceptible to desorption, particularly if highly charged or hydrophilic molecules are bonded.^{20–22} In connection with this, stability is important not only for the immobilization of the recognition element but also for the incorporation of antifouling entities (e.g., PEG, zwitterionic polymers, among others).^{23,24} Thus, the lack of a strategy to avoid the desorption of these elements may lead to 2D material-based biointerfaces that are unsuitable for biosensing applications. Although multipyrene heterobifunctional cross-linkers were demonstrated to efficiently link biomolecules on graphene with better stability,²⁵ these molecules are not commercially available, and their obtention

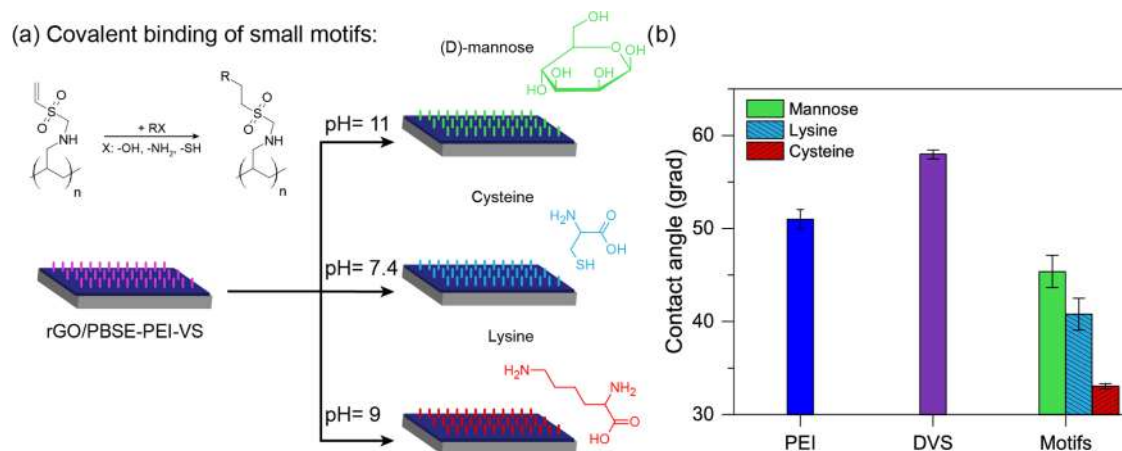


Figure 2. (a) Scheme of the covalent binding of small motifs to PEI–VS substrates. (b) Contact angle values at different functionalization steps of PEI 750 kDa-modified substrates. The error bars represent the 95% confidence interval.

requires several complex steps, which lead to difficulty in their mass production.

On the other hand, it has been demonstrated that 2D material-based devices do not necessarily require setting the recognition elements in direct contact with the semiconducting nanomaterial for achieving the transduction mechanism. This is because the electric field decay length can be strongly extended by the integration of polymers such as PEG-brushes^{26,27} or polyelectrolyte multilayers^{28,29} to the interface. In this sense, the construction of heterobifunctional supramolecular-covalent polymer scaffolds may be an attractive approach to robustly bond different desired elements. Although noncovalent immobilization strategies have been reported for the integration of enzymes with polyelectrolytes,^{30,31} there is still a lack of a general approach for anchoring affinity recognition elements (e.g., antibodies, aptamers, etc.) and antifouling building blocks, both of which are key components for the generation of sensing devices in biological samples.

Here, we describe the design and synthesis of vinylsulfonated-polyamine (PA-VS) scaffolds suitable for the immobilization of both recognition (lectins and antibodies) and antifouling elements (PEG) on graphene surfaces. These heterobifunctional scaffolds were constructed by three simple surface modification steps: (i) the adsorption of pyrenebutanoic acid succinimidyl ester (PBSE) on graphene; (ii) the fast reaction of polyamines in aqueous solutions with surface-bound PBSE, yielding a multipoint attached film through pyrene groups; and (iii) the modification of the remaining primary amine groups with divinylsulfone (a well-known cross-linker of –SH, –NH₂, and –OH groups via Michael type addition^{32–34}), yielding PA-VS on graphene. The step-by-step construction of the heterobifunctional coating was monitored by spectroscopic ellipsometry and contact angle measurements. Vinylsulfonation of polyamines was proved by Raman spectroscopy, and its reactivity towards hydrophilic molecules containing –SH, –NH₂, or –OH groups was demonstrated by contact angle measurements. Furthermore, the conservation of the semiconducting properties of the underlying graphene was evaluated by recording the features of the field-effect transistors (FETs) after the modification by PA-VS scaffolds. Later, the attachment of recognition elements to PA-VS was firstly optimized for concanavalin A (ConA), a model lectin with a high affinity to glycans. The stability of the architecture

in surfactant-containing media, its antifouling properties, and the recognition of a glycoprotein were studied by spectroscopic ellipsometry and surface plasmon resonance (SPR) spectroscopy. Finally, the specific recognition of SARS-CoV-2 spike protein and human ferritin by two different scaffolds containing the respective monoclonal antibodies (mAbs) was studied by SPR. These target molecules are of major importance for the rapid detection and monitoring of COVID-19-affected people. Both K_D equilibrium constant determination and regeneration studies on these functionalized surfaces were also performed.

2. METHODS

2.1. Heterobifunctional Scaffold. Supramolecular scaffolds of vinylsulfonated-polyamines (PA-VS) on graphene-covered surfaces (obtained as previously reported^{28,30}) were prepared by sequential surface modification steps: (i) Substrates modified by reduced graphene oxide (rGO) were incubated in 5 mM 1-pyrenebutanoic acid succinimidyl ester (PBSE) in dimethylformamide (DMF) for 2 h (see the scheme in Figure 1a). Then, the substrates were washed with DMF and dried. (ii) PBSE-modified graphene substrates (hereafter rGO/PBSE) were then incubated in 2 mg/mL poly(allylamine hydrochloride) (PAH) or poly(ethyleneimine) (PEI) at pH = 10 for 1 h, washed with deionized water, and dried (Figure 1b). (iii) The PA-VS scaffolds (hereafter rGO/PBSE-PA-VS) were obtained by incubating the polyamine-modified rGO/PBSE substrates in 5% divinylsulfone (DVS) solution in carbonate buffer (0.5 M Na₂CO₃, pH = 11) for 1 h, washed with deionized water, and dried (Figure 1c).

2.2. Binding of Small Motifs to rGO/PBSE-PA-VS Substrates.

(a) Mannose binding (through –OH groups) was performed by incubating the substrates in a 10 wt % mannose solution in carbonate buffer (0.5 M Na₂CO₃, pH = 11) for 18 h. (b) Cysteine (Cys) binding (through –SH groups) was performed by incubation of the substrates in 10 mM L-cysteine in PBS (pH = 7.4) for 12 h. (c) Lysine (Lys) binding (through –NH₂ groups) was carried out by incubation of the substrates in 10 mM L-Lysine in borate-buffered saline solution (BBS, 10 mM sodium borate, 140 mM NaCl pH = 9.0) for 12 h (see the scheme in Figure 2a). The substrates were finally washed with Milli-Q water and dried.

2.3. Covalent Binding of Lectins and Antibodies to rGO/PBSE-PEI-VS.

(i) The substrates were incubated in 100 μg/mL protein solution in BBS buffer (pH = 9.0) for 5 h (at this pH, both Cys and Lys residues present in the protein react covalently with PEI–VS) and then washed with BBS. (ii) For the incorporation of the antifouling properties, the substrates were then incubated in 0.2 mM PEG-NH₂ (10 kDa) solution in BBS (pH = 9.0) for 2 h and washed with BBS. (iii) The substrates were finally incubated in 100 mM

ethanolamine (ETA) solution in BBS (pH = 9.0) for 30 min to block the remaining vinyl sulfone groups,³⁵ washed with BBS, and stored in buffer.

The PEI-VS scaffold approach was compared to the usual monopyrene modification method widely reported in the literature:^{8,16,18,19,21,25} Briefly, rGO/PBSE substrates were incubated in 100 $\mu\text{g}/\text{mL}$ protein solution in PBS (pH = 7.4) buffer for 1.5 h. Then, the substrates were incubated in 0.2 mM PEG-NH₂ (10 kDa) in PBS (pH = 7.4) for 2 h and finally incubated in 100 mM ETA solution in PBS (pH = 7.4) for 15 min, washed with BBS, and stored in PBS.

2.4. Surface Plasmon Resonance (SPR) Spectroscopy. A basic piranha solution at 60 °C (NH₄OH 35% and H₂O₂ 30% 1:1) was used to clean SPR102 Au substrates (BioNavis) for 10 min. The SPR substrates were first modified with cysteamine and then with rGO as previously reported.^{28,36} The rGO-modified substrates were washed with water and dried with N₂. A multiparametric surface plasmon resonance (MP-SPR) instrument, SPR Navi 210 A (BioNavis Ltd., Tampere, Finland), was used to monitor the sequential processes for protein functionalization, and their affinity to the target molecules. SPR measurements were carried out using a 670 nm laser and a flow rate of 20 $\mu\text{L}/\text{min}$. Time-resolved SPR responses were fitted with TraceDrawer software to obtain association (k_{ass}) and dissociation (k_{diss}) kinetic constants and the effective dissociation equilibrium constant ($K_{\text{D}} = k_{\text{diss}}/k_{\text{ass}}$). The software corrected small TIR matrix differences by comparison with the buffer (appreciated as sharp falls in the fitted curves). Each system was measured and analyzed in duplicate. Surface mass density estimation was performed as described elsewhere,³⁷ using a $d\eta/dC$ value of $1.77 \times 10^{-10} \text{ cm}^3 \text{ ng}^{-1}$. The regeneration of the interface for antibody-antigen recognition was carried out by elution of 10 mM glycine (Gly) pH = 2.0 for 2 min.

2.5. Raman Spectroscopy. Raman spectra were acquired using an i-Raman BW415-532S (BWTek) Raman spectrometer. The excitation wavelength was 785 nm (power = 395 mW) and the laser was focused on the substrates by an optical microscope (BAC151B, BWTek).

2.6. Spectroscopic Ellipsometry. Ellipsometric measurements were done using an α -SE (J.A. Woollam) ellipsometer with a rotating compensator and CCD detector. Measurements were performed for the entire spectral range (380–900 nm, 180 wavelengths) at three angles of incidence (65°–70°–75°), using a collimated beam (~3 mm). Setup alignment and lamp intensity were checked before every measurement. Each sample was analyzed at least at two different spots, using the high-precision alignment routine and a long acquisition time. All measurements were performed in air, on dried samples. Unless otherwise stated, all ellipsometric models were fitted for the entire spectral range.

2.7. Contact Angle. Measurements were done with a Ramé-Hart System model 290 in a static-drop setup. Two drops of Milli-Q water (1 μL) were analyzed for each sample.

2.8. Field-Effect Measurements of Graphene Transistors (GFETs). Electrolyte-gated graphene field-effect transistors with an Ag/AgCl gate (model GFET-GB10) were supplied by GISENS BIOTECH (Argentina). Electrical measurements were performed by utilizing a FET measurement station Zaphyrus-W10 (GISENS BIOTECH, Argentina). For the acquisition of GFET transfer characteristic curves, the current between the source and drain electrodes (I_{DS}) was measured as a function of the gate potential (V_{G}), while the potential between the drain and the source (V_{DS}) was fixed at 100 mV. Field-effect experiments were performed in 200 μL of 10 mM HEPES buffer and 100 mM KCl (pH = 7.4). Charge neutrality point V_{CNP} and transconductance ($[dI_{\text{DS}}/dV_{\text{G}}]/V_{\text{DS}}$) were obtained from the transfer curves.

3. RESULTS AND DISCUSSION

3.1. Construction of Vinylsulfonated-Polyamines (PA-VS) Heterofunctional Scaffolds. After PBSE modification (Figure 1a), polyamines were attached to the surface by the reaction of their amino groups with the succinimide group from PBSE (Figure 1b). Particularly, low- and high-molecular-

weight (M_{w}) PAH (17.5 and 140 kDa) and PEI (25 and 750 kDa) were used. The step-by-step surface functionalization was monitored by spectroscopic ellipsometry (SE), as it is a highly sensitive, nondestructive, and reliable technique for determining thin-film thickness. An ellipsometric model was constructed for rGO substrates and their modification with PBSE, as described in the Supplementary Information file (SI). Then, an optical model was built for analyzing the ellipsometric results from the functionalized rGO/PBSE surfaces. For the construction of the optical model, a Cauchy layer was introduced on top of the rGO layer, and its thickness was adjusted until it became optimally fit.

As can be seen from the thickness evolution of the Cauchy layer in Figure 1d, both polyamines are being successfully deposited on the rGO/PBSE surface. However, the use of PEI allows for a thicker coating layer compared with PAH. As expected,³⁸ M_{w} impacts on the thickness of the PA layer, yielding thicker deposited PA layers for higher M_{w} polymers. Complementary characterization of the surface modifications by contact angle (CA) measurements was also performed (Figure 1e).

CA measurements reveal that PBSE is being anchored to rGO, as a decrease in the contact angle by 7.4% (from $78.8 \pm 0.7^\circ$ to $73.0 \pm 0.5^\circ$) is observed. Furthermore, the integration of the polyamines is also confirmed by a decrease in the CA. In addition, a more efficient coverage could be ascribed to the functionalization with PEI as compared with PAH. Whereas the modification with PAH decreases the CA just by ~5%, the modification with PEI leads to a marked decrease of the CA of almost 30%.

As previously mentioned, divinylsulfone (DVS) has proved to be a suitable chemical tool for surface modification, allowing the cross-linking of different biological molecules with high efficiency and resistance towards hydrolysis. Therefore, PA films were then exposed to DVS, allowing the $-\text{NH}_x$ groups to react with the vinylic groups from DVS, as depicted in Figure 1c. The thickness of the PA-VS layer was estimated by SE, adjusting the thickness of the previous Cauchy layer. As can be seen in Figure 1d, none of the PA layers seems to detach from the rGO/PBSE surface after treatment with DVS. Contrarily, the ellipsometric response of the platform suggests an effective thickness increase of the layer. These effects are more notorious in the case of PEI films, also evidencing the coverage differences between both polyamine platforms. Moreover, CA values increased considerably after DVS reaction (except for PAH 140 kDa), which proves the success of the functionalization step (Figure 1e).

Taking advantage of the high hydrophilicity of glycosylated surfaces, the functionalization with mannose (mannosylation) was used as a strategy for proving the reactivity and degree of modification of the vinylsulfonated-polyamine scaffolds.^{39,40} As displayed in Figure 1d, no desorption of the previously assembled platform is observed after the mannosylation procedure as the ellipsometric thickness of the whole coating remains almost the same. In terms of the CA values, however, there is a clear decrease after mannosylation. Furthermore, the substrate modified with PEI 750 kDa exhibits the greatest surface hydrophilic character after the incubation in mannose ($45.4 \pm 1.7^\circ$), suggesting a higher degree of functionalization. Then, based on the above-mentioned results, PEI 750 kDa was chosen for the preparation of vinylsulfonated-polyamine scaffolds to further study the binding of small chemical motifs, lectins, and antibodies.

To further confirm the reaction of DVS with amine groups of PEI, Raman spectroscopy measurements were performed. As described in SI, a volume of PEI dispersion was mixed with DVS for 1 h and then purified. Raman spectra of pure DVS and PEI and PEI-modified samples are shown in Figure 1f. Typical peaks for PEI and DVS are observed in their respective spectra, while both sets of peaks are present in the PEI-VS sample, indicating a successful reaction. Furthermore, the peak assigned to the symmetric C-S stretching, which is observed at 714 cm^{-1} for DVS, shifts to 674 cm^{-1} in the PEI-VS composite. This shift towards lower wavenumbers confirms that the reaction between the vinylic moieties from DVS and the amine groups from PEI effectively takes place. Table S2 summarizes the peak assignments for the three samples.

3.2. Covalent Binding of Small Motifs to PEI-VS Scaffolds. Surface covalent cross-linking of biomolecules such as proteins, DNA, and other recognition elements is typically performed through specifically and carefully chosen chemical groups to ensure the biomolecule functionality. In this regard, vinyl sulfone (VS) chemistry is particularly attractive due to its reaction selectivity, as the VS group specifically reacts with $-\text{SH}$, $-\text{NH}_2$, or $-\text{OH}$ groups depending on the pH value,^{39,41} ending the covalent cross-linking to particular biomolecule sites.^{32,42,43}

Therefore, those reactions were employed to covalently attach different chemical motifs, such as mannose (through $-\text{OH}$ groups), cysteine (through $-\text{SH}$ groups), and lysine (through $-\text{NH}_2$ groups) to the rGO/PBSE-PEI-VS scaffolds. To this end, the heterofunctional scaffolds were incubated in mannose, lysine, or cysteine solutions (Figure 2a), which yielded a marked decrease in the contact angle ($45 \pm 2^\circ$ for mannose, $40 \pm 2^\circ$ for cysteine, and $33.0 \pm 0.3^\circ$ for lysine) as shown in Figure 2b. In all cases, a noticeable increase in the hydrophilicity of the surface is evidenced, owing to the hydrophilic character of the linked moieties, confirming the chemical modification of the surface and displaying the versatility of the fabricated architecture. It is worth noting that no significant difference in the coating thickness after each modification was observed by ellipsometry (see SI, Figure S2).

3.3. In Situ PEGylation: Stability of PEG Interfaces on Graphene. One of the most commonly used strategies for imparting adhesion resistance to nonspecific biomolecules involves the functionalization of surfaces with poly(ethylene glycol) (PEG).⁴⁴ In fact, this element has provided excellent antifouling features to graphene-based biosensors.^{18,26} Therefore, the covalent modification of the PEI-VS coatings with PEG (PEGylation) was also studied as shown in Figure 3a. The results in Figure 3b correspond to the *in situ* PEGylation of rGO/PBSE-PEI-VS monitored by surface plasmon resonance (SPR) spectroscopy. Consecutive injections of 0.2 mM PEG-NH₂ solution (12 min) followed by a buffer injection (3 min) were performed. The time evolution of the minimum reflectivity angle (θ_{SPR}) of the SPR sensor is presented in Figure 3b. As shown in the sensorgram, θ_{SPR} increases sequentially with the number of PEG-NH₂ injections (highlighted by a dashed line in the sensorgram), which indicates an increase in coating thickness. A thickness of approximately 2 nm after three injections was estimated. Since the most common strategy to attach antifouling elements to graphene-based sensors is through monopyrene linkers, the PEGylation of unmodified rGO/PBSE substrates was comparatively studied (Figures 3c and S3).⁴⁵ For the rGO/PBSE system, a large increase of θ_{SPR} was observed during the first

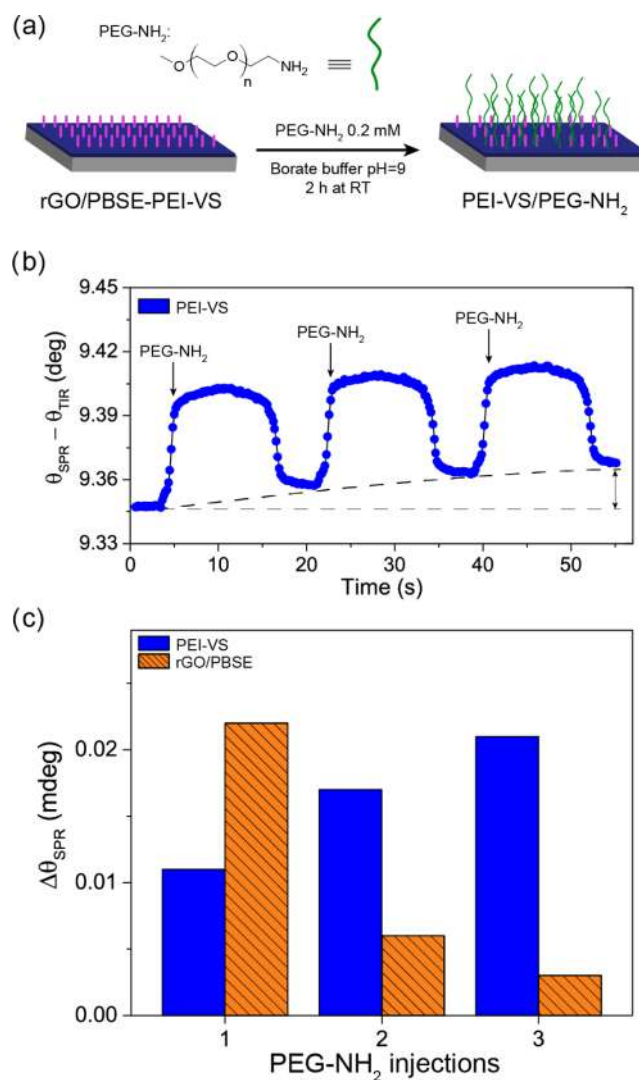


Figure 3. (a) Schematic representation of PEI-VS PEGylation. (b) SPR sensorgrams for the PEGylation of PEI-VS-modified graphene sensors. The dashed line serves as an eye guide for appreciating the PEGylation. (c) Change of θ_{SPR} as a function of the number of injections determined in the buffer media for rGO/PBSE-PEI-VS (solid bars) and rGO/PBSE (patterned bars).

PEG-NH₂ injection. However, an important and non-recoverable PEG mass loss occurred during the washing step with buffer and even after the following two PEG-NH₂ injections. This desorption of PEG linked to PBSE is in agreement with previously reported observations for monopyrene molecules on graphene.^{20–22,25} Thus, it is evidenced that construction of the PEI-VS scaffold on the rGO/PBSE surface effectively prevents the coating desorption after the PEGylation step, resulting in more stable functional surfaces.

3.4. Covalent Cross-linking of Proteins and Subsequent PEGylation of PEI-VS Scaffolds. Having shown that the vinylic groups of PEI-VS scaffolds are selectively reactive to a variety of chemical moieties, the covalent cross-linking of biomacromolecules was also explored. The subsequent PEGylation of the protein-modified PEI-VS architecture was studied as a strategy for conferring antifouling properties to the whole scaffolds. As a model system, the anchoring of Concanavalin A (ConA, a well-known lectin protein with high lysine content and no cysteine residues⁴⁶) was first

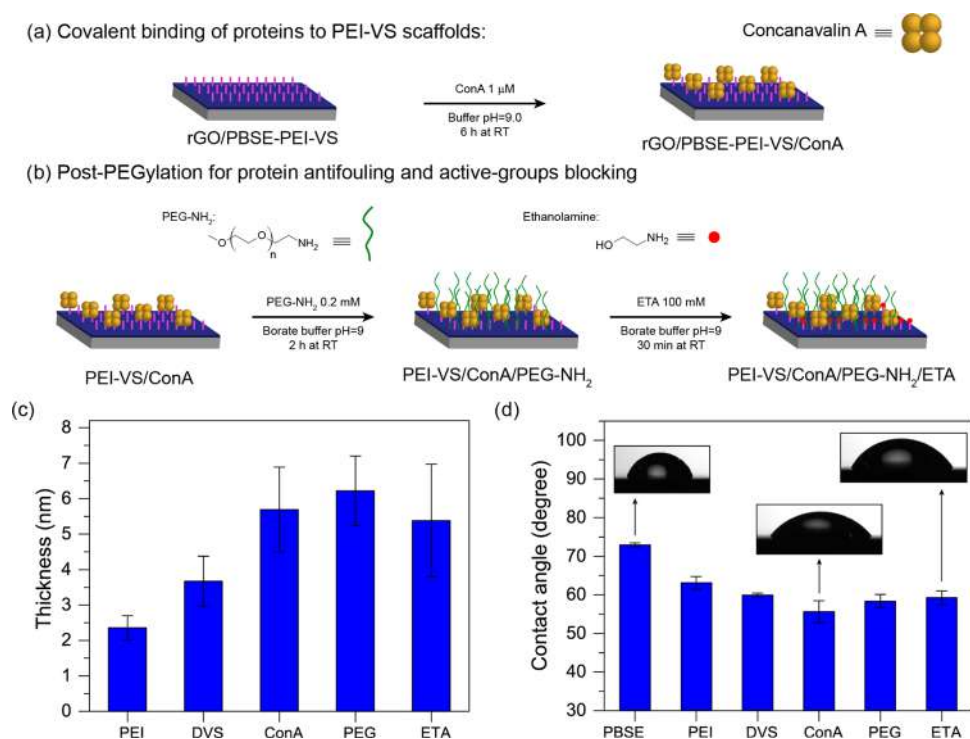


Figure 4. Schematic representation of the covalent binding of ConA on PEI-VS scaffolds (a) and later PEGylation and blocking with ETA (b). Thickness (c) and contact angle values (d) after each modification step of rGO/PBSE substrates. Bars represent the 95% confidence interval.

performed, followed by reaction with PEG-NH₂ and deactivation of the remaining VS groups by treatment with ethanolamine (ETA) solution, as schematized in Figure 4a,b.

The step-by-step covalent modification of PEI-VS scaffolds with ConA, PEG-NH₂, and ETA was monitored by SE and CA measurements. As can be seen from Figure 4c,d, a thickness increase of approximately 2 nm and a CA decrease of approximately 5° were observed after ConA binding. Furthermore, a thickness increase of approximately 0.5 nm was observed after the PEGylation step of the PEI-VS/ConA substrates. Finally, after blocking the remaining VS groups with ETA, a film thickness decrease of 0.8 nm was observed. In addition, the evolution of the CA confirms the successful integration of each component into the supramolecular scaffold.

The covalent modification of PEI-VS scaffolds with ConA, PEG-NH₂, and ethanolamine (ETA) was also studied by *in situ* SPR. As can be seen in the SPR sensorgrams depicted in Figure S4, more than 95% of the protein was attached to PEI-VS scaffolds during the first 40 min. Nevertheless, as the covalent reaction to lysine groups is relatively slow,³⁹ the incubation of PEI-VS scaffolds in the protein solution was maintained during 5 h (Figure S4). PEGylation was performed afterwards, showing a slight increase of the θ_{SPR} signal and confirming the SE results discussed above. Direct protein cross-linking on unmodified rGO/PBSE sensors was comparatively studied (see the SI file).

The estimated ConA surface mass density values are in the range of 350–440 ng/cm² for PEI-VS and PBSE systems (Figure S5). These values obtained for graphene-modified SPR sensors are slightly higher than those obtained for Au SPR sensors without graphene.^{47–51} This observation may be explained in terms of the higher surface area caused by graphene flakes, in agreement with other reports.^{52,53} However,

when employing the monopyrene approach, a decrease of θ_{SPR} is observed during the PEGylation and ETA steps, suggesting some protein-PBSE desorption. Therefore, once again, the architecture built by ConA cross-linking to PEI-VS scaffolds proves to be more stable than that produced directly on PBSE.

3.5. Stability of the Architecture, Antifouling Capabilities, and Specific Recognition. Time stability in the sensing media is a prerequisite of any interfacial architecture developed for use in sensing devices. Therefore, the stability of the PEI-VS/ConA/PEG-NH₂ scaffolds was studied in surfactant-containing solutions.

Although the new covalent bonds formed after each modification step are not likely to be cleaved in operative conditions, the whole system stability relies on the noncovalent multivalent π - π interactions between graphene and PBSE-modified PEI. Having this in mind, to study the stability of the whole architecture, the PEI-VS/ConA/PEG-NH₂ scaffolds were incubated in a solution of the nonionic surfactant Triton X-100 (0.2% in the same buffer used for the assembly), and the changes in the thickness of the film were monitored by SE at different time intervals during 24 h.

For each measurement, the substrates were rinsed with the appropriate buffer and dried. As shown in Figure 5a, no significant thickness changes are observed after the surfactant treatment (differences are within the deviation of the measurements), suggesting that no desorption of the film components occurs and demonstrating the good stability of the whole architecture.

Another crucial aspect for the proper use of the present scaffolds in biosensing applications is the antifouling behavior of the interface. To evaluate the antifouling performance, the nonspecific adsorption of bovine serum albumin (BSA) on different interfaces was comparatively studied as a model of fouling. As a reference, the adsorption on rGO-coated

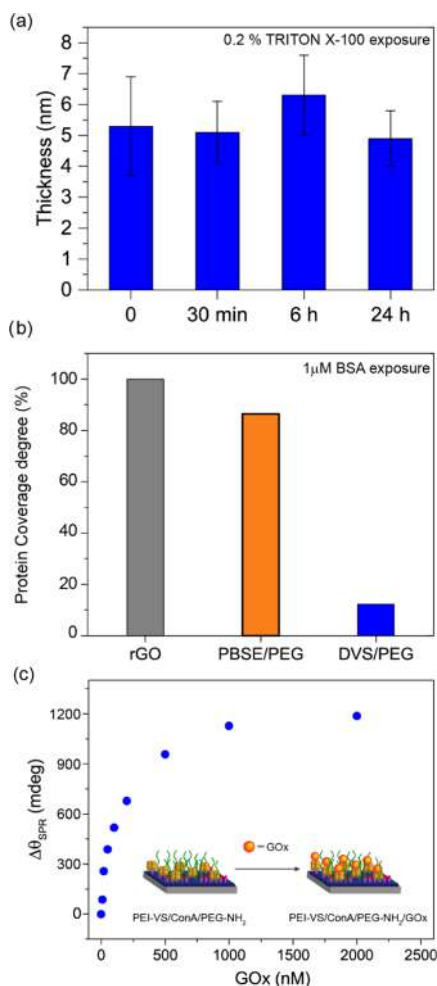


Figure 5. (a) Structural stability of PEI-VS/ConA/PEG-NH₂ scaffolds in terms of the ellipsometric thickness after incubation in Triton X-100 solutions for increasing soaking times. Bars represent the 95% confidence interval. (b) Antifouling capacity of the PEGylated scaffold compared with rGO and PBSE substrates. (c) Steady-state θ_{SPR} response as a function of the glucose oxidase (GOx) concentration for PEG-ConA-VS-PEI scaffolds.

substrates was first determined by exposing the rGO surfaces to 1 μM bovine serum albumin (BSA) solution in BBS (pH = 9) for 30 min, rinsing with BBS and deionized water, and drying. The nonspecific interaction of BSA with rGO was monitored by SE measurements.

After adsorption, a Cauchy layer of 1.88 nm was fitted. This thickness value is consistent with the formation of a monolayer coverage for this protein,⁵⁴ and it was used to estimate the protein coverage degree of the other surfaces. In the case of PEGylated rGO/PBSE substrates (previously deactivated by ETA), the adsorption of BSA corresponds to 85% of the amount of protein adsorbed on rGO (Figure 5b). Contrarily, PEGylated PEI-VS substrates (also deactivated by ETA) exhibited coverage values of just 12% of the coverage observed in rGO substrates. Clearly, the strategy employing the rGO/PBSE-PEI-VS/PEG-NH₂ architecture leads to superior antifouling properties of the surface.

Having shown the structural stability and antifouling capability of the PEGylated PEI-VS scaffold, the recognition capacity of the covalently bound biomacromolecules was studied. To this end, the biological affinity between the cross-

linked lectin ConA (a carbohydrate-binding protein) and glucose oxidase^{49,55} (GOx, a model protein with a high content of carbohydrate residues) was evaluated *in situ* by SPR. Solutions of increasing GOx concentrations were injected at 20 $\mu\text{L}/\text{min}$ and monitored by employing SPR sensors modified with the rGO/PBSE-PEI-VS/ConA/PEG-NH₂ architecture. The steady-state increment of the minimum reflectivity angle ($\Delta\theta_{\text{SPR}}$)⁵⁶ was obtained as a function of the GOx concentration,⁵⁶ as shown in Figure 5c. By fitting these values to a simple binding equation (eq S1), the effective dissociation constant was estimated to be $K_{\text{D}} = 134 \pm 18$ nM, in good agreement with the ConA-GOx affinity constants reported by other authors, demonstrating that cross-linked ConA retains its recognition ability when integrated to the PEI-VS scaffolds, even after PEGylation.⁵⁷

3.6. Semiconducting Properties of the Underlying Graphene. To demonstrate that the construction of the heterofunctional scaffolds does not disrupt the semiconducting properties of graphene, the construction of a PEI-VS scaffold and its binding to ConA and PEG-NH₂ were performed on the graphene channel of GFETs. The transfer characteristic curves after each modification step were recorded in HEPES buffer at pH 7.4. Figure 6 summarizes the results for the relevant

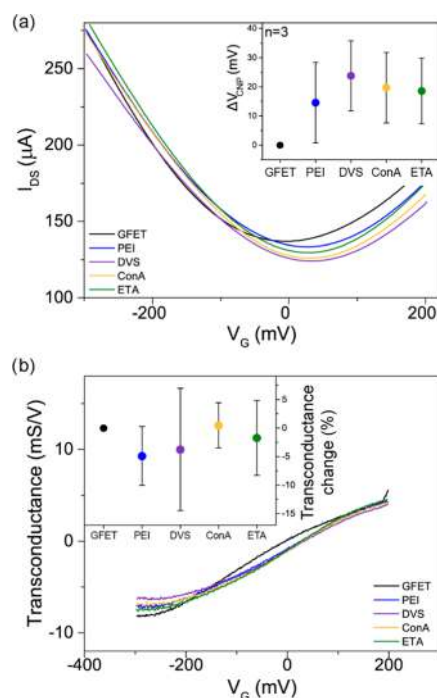


Figure 6. (a) Transfer characteristic curves for a GFET before and after each modification step for the preparation of PEI-VS and its binding to ConA, PEGylation, and blocking. Inset: Shift of the charge neutrality point (ΔV_{CNP}) as a function of the successive modifications for a set of three GFETs. (b) Transconductance as a function of V_{G} for the characteristic transfer curves shown in (a) and its percentual change (inset).

parameters of the field-effect study. Minor changes in both the voltage of the charge neutrality point (ΔV_{CNP}) (Figure 6a) and transconductance ($[dI_{\text{DS}}/dV_{\text{G}}]/V_{\text{DS}}$) values (Figure 6b) were detected after each functionalization step. These results indicate that the integration of the different components on the graphene channel does not modify its semiconducting properties. Thus, the construction of the PEI-VS scaffolds

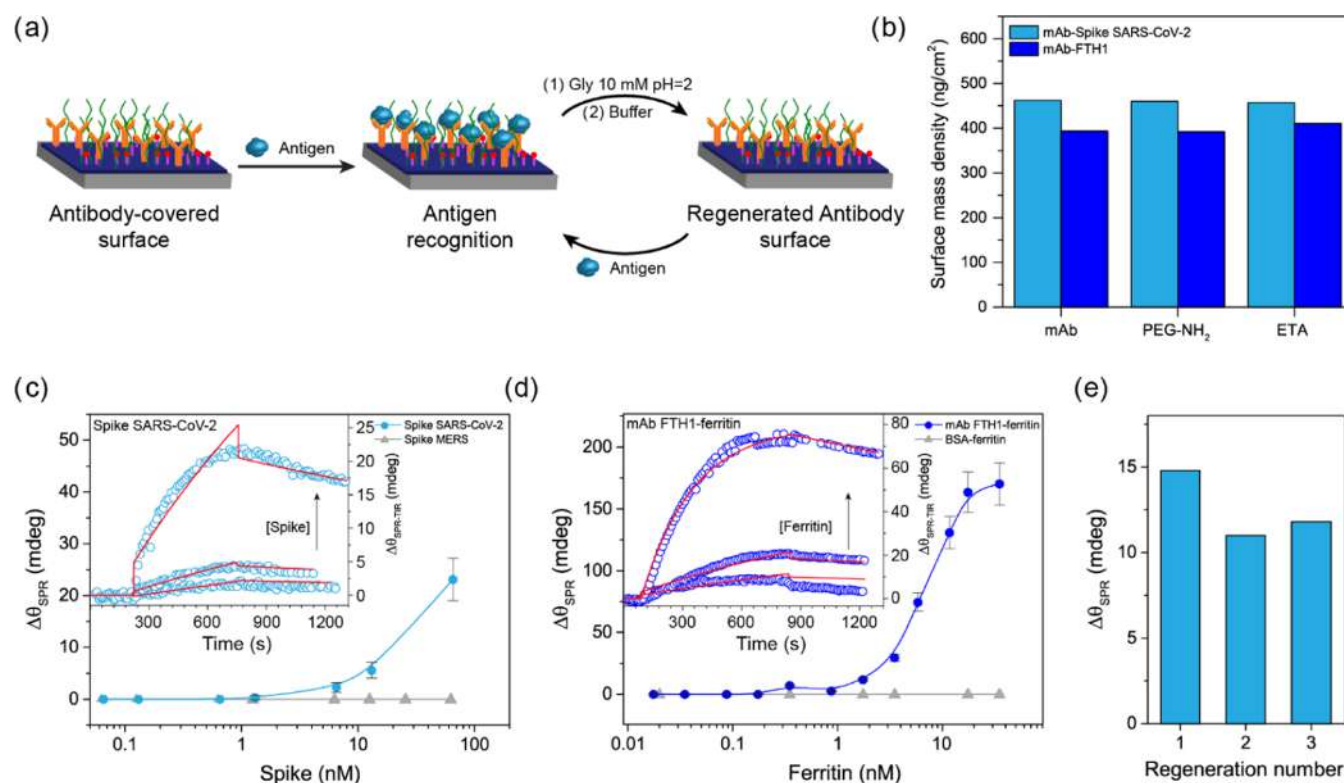


Figure 7. (a) Scheme of antigen capture and regeneration of the antibody-covered PEI-VS scaffolds. (b) Surface mass density after each modification step for VS-PEI/rGO-SPR sensors. (c) Steady-state SPR response ($\Delta\theta_{\text{SPR}}$) as a function of SARS-CoV-2 (circles) and MERS (triangles) spike protein concentrations for VS-PEI scaffolds modified with spike protein. Inset: Kinetic SPR response during the elution of 6.53, 13.07, and 65 nM SARS-CoV-2 S1 protein for the same sensor. Association and dissociation best fits are plotted with solid lines. (d) θ_{SPR} response as a function of the human ferritin concentration for VS-PEI scaffolds modified with mAb-FTH1 (circles) or BSA (triangles). Inset: Kinetic SPR response during the elution of 1.74, 3.5, and 35 nM human ferritin for the same sensor. (e) SPR response to SARS-CoV-2 S1 protein after every three regenerations of the biointerface.

becomes compatible with the development of biosensing platforms based on GFETs.

3.7. Covalent Binding of Antibodies to PEI-VS Scaffolds for Antigen Recognition. To evaluate the suitability of the PEI-VS scaffolds for the development of graphene-based affinity biosensors, two different antibody-antigen pairs were tested. For these studies, monoclonal antibodies (mAbs) against SARS-CoV-2 spike protein (mAb-SARS-CoV-2 spike, Sino Biological Inc., catalog number: 40150-R007) and human ferritin (mAb-FTH1, Sino Biological Inc, catalog number: 13217-MM06) were covalently bound to the PEI-VS scaffold on rGO-modified substrates (Figure 7a). Both SARS-CoV-2 spike and human ferritin have become proteins of huge relevance in the context of the COVID-19 pandemic. On one side, the spike protein of the SARS-CoV-2 virus is an antigen of paramount importance for ultrarapid COVID-19 diagnosis in nasopharyngeal swab or saliva samples.^{8,11,58} On the other hand, serum ferritin level increase is associated with a higher probability of developing or continuing a cytokine storm in COVID-19 patients.⁵⁹ Thus, ferritin is considered a good indicator of the COVID-19 inflammatory response, and its value can be used to perform an assessment of the clinical progress and provide alertness on critical patients.^{10,60}

The covalent modification of PEI-VS scaffolds with mAb-SARS-CoV-2 or mAb-FTH1, followed by PEG-NH₂ and ETA modifications, was monitored by SPR. A surface coverage of 436 ± 30 ng/cm² was estimated from SPR measurements

(Figure 7b), and the interfacial architecture exhibited excellent stability to remain stable after PEGylation and ETA deactivation steps. Contrarily, experiments performed directly on the rGO/PBSE substrates revealed noticeable coating desorption during post-treatment with PEG-NH₂ and ETA (Figure S6), reinforcing the advantages of employing the PEI-VS functionalization approach.

The recognition of the SARS-CoV-2 spike protein by the mAb-SARS-CoV-2-modified PEI-VS platform was also studied by SPR. Solutions of increasing concentration of Wuhan SARS-CoV-2 S1 protein (Sino Biological Inc., catalog number: 40591-V08H, accession number YP_009724390.1) were injected and the obtained steady-state $\Delta\theta_{\text{SPR}}$ values are shown in Figure 7c, as a function of the protein concentration. Analogous experiments were carried out employing MERS spike protein as a control (also depicted in Figure 7c). SPR results indicate that the mAb-SARS-CoV-2-modified PEI-VS platform has a suitable specificity against SARS-CoV-2 S1, whereas no recognition was observed for the MERS S1 protein. The affinity profile is in good agreement with previously reported ELISA measurements employing the same reagents.⁸ Both association ($k_{\text{ass}} = 6.74 \times 10^3 \text{ M}^{-1} \text{ s}^{-1}$) and dissociation ($k_{\text{diss}} = 3.26 \times 10^{-4} \text{ s}^{-1}$) kinetic constants and K_{D} were estimated from the analysis of the time-resolved binding curves (Figure 7c inset). The obtained dissociation constant value ($K_{\text{D}} = 48.4$ nM) indicates an affinity in the same range as those reported for the interaction of human angiotensin-converting enzyme 2 (hACE2) with SARS-CoV-2 S1 ($K_{\text{D}} = 94.6$ nM⁶¹),

SARS-CoV-2 spike ($K_D = 1.2\text{--}15\text{ nM}^{62,63}$), and SARS-CoV-2 RBD (4.7 nM^{64}). It is worth noting that our K_D value implies that the present construction would become suitable for the development of rapid detection platforms for SARS-CoV-2 antigens.^{58,65}

A K_D value of 42 nM was obtained for SARS-CoV-2 S1 and the mAb immobilized with the PBSE approach (Figure S7). The similarity of the K_D values suggests that the VS-PEI scaffold does not compromise the affinity between mAb and S1 to a greater extent than the PBSE method. Since the used mAb neutralizes also the RBD protein (see Materials Section of the SI), a binding event through the RBD is the most likely scenario. As RBD groups can present variations for different SARS-CoV-2 mutations, the used mAb may display some affinity energy changes for the virus variants. In this regard, the high versatility of the VS-PEI scaffold would enable also the covalent binding of mAbs specially developed for the new variants.

In addition, the recognition of human ferritin by the rGO/PBSE-PEI-VS sensors modified with mAb-FTH1 was also studied by SPR (Figure 7d). A high affinity of ferritin with the interface was found, while no recognition was observed for a sensor modified with BSA, employed as a control. From the fit of the time-resolved binding curves (Figure 7d inset), the derived constant values are $k_{\text{diss}} = 2.60 \times 10^{-4}\text{ s}^{-1}$, $k_{\text{ass}} = 1.02 \times 10^5\text{ M}^{-1}\text{ s}^{-1}$, and $K_D = 2.54\text{ nM}$. Since COVID-19 patients with poor clinical progress present ferritin serum values higher than $400\text{ }\mu\text{g/L} = 0.84\text{ nM}$ (i.e., hyperferritinemia), and those severely ill higher than 3 nM ,⁶⁰ the mAb-FTH1-modified architecture becomes a promising alternative platform for the development of rapid ferritin diagnostics based on graphene sensors. For instance, the platform could be used for the clinical discrimination of COVID-19 patients in terms of their ferritin level ranges (e.g., normal levels, hyperferritinemia, and severe cytokine storm; see Figure S8). This information is useful to predict disease severity and the extent of the cytokine storm, and therefore, to tailor the treatment strategy.^{59,66}

Finally, the regeneration of the mAb recognition sites after the binding of antigens was also studied. SPR results show that incubation in glycine 10 mM (pH = 2) for 2 min is a suitable regeneration treatment, as the initial SPR signal was recovered even after three binding-regeneration cycles (Figure 7e).

4. CONCLUSIONS

Herein, we have shown that the sequential construction of PBSE-PA-VS scaffolds yields robust supramolecular coatings on graphene anchored by $\pi\text{--}\pi$ interactions with multiple pyrene groups. Particularly, the PEI-VS scaffold has been proved to allow the suitable covalent linking of different small motifs, lectins, and antibodies. By exploring the pH dependence of the VS moiety reactivity, selective functionalization by covalent cross-linking to different chemical groups was demonstrated. Moreover, PEI-VS scaffolds can be endowed with antifouling capabilities by the covalent integration of short-length PEG chains. Furthermore, the whole PBSE-PEI-VS scaffolds become more stable towards post-functionalization treatments in comparison with the widely employed monopyrene modification approach. Thus, PEGylation provides antifouling capabilities without hampering the specific recognition between surface-anchored biomacromolecules and target molecules, as in the case of Concanavalin A-Glucose oxidase interaction. Finally, we have also proved that the construction of PEI-VS-based scaffolds does not disrupt the

band structure of graphene, keeping its semiconducting properties.

The potential of the PEI-VS-based scaffolds in affinity biosensing platforms was illustrated by integrating monoclonal antibodies against SARS-CoV-2 spike protein and human ferritin, which allowed for the selective and accurate binding of these relevant antigen proteins related to the COVID-19 pandemic in lab-made solutions. The K_D values obtained for these antigen-antibody-based recognition strategies in synthetic samples are within a range that becomes promissory for the construction of sensors operating in real clinical samples for the rapid detection of SARS-CoV-2 infections and for monitoring the health state of patients transiting the COVID-19 disease. For application in a real device, further tests for evaluating the functionalized GFET performance in biological samples such as human serum or saliva are required together with proper positive and negative controls, cutoff reading, sensitivity, and specificity determination in real complex matrices. However, the present results constitute a solid basis for deeper studies concerning not only COVID-related antigens but also other relevant biomarkers by conjugating the suitable recognition elements using this functionalization methodology for the construction of GFET-based sensors. In this regard, compared with conventional immunoassays such as ELISA or lateral-flow test, graphene FET sensing devices prepared with the heterofunctional VS-PA scaffolds for the anchoring of recognition and antifouling elements with covalent-like stability could have the following advantages: (i) The present detection strategy needs just one recognition element (e.g., a capture mAb), whereas the commonly used ELISA and lateral-flow test require the use of capture Abs, detector Abs, and enzymes or nanoparticles for the readout. (ii) The target molecule recognition and, therefore, the sensor response would be faster than the ELISA methodology that requires sample incubation, washing steps, incubation in solution with enzyme linked to detector Ab, enzymatic reaction, and a readout step. (iii) The activity of the mAb covalently bound to VS-PEI on graphene could be regenerated for reusing a feature that is not possible in lateral-flow tests.

We envision this heterobifunctional supramolecular-covalent approach will contribute to the development of novel rapid, reproducible, sensitive, and scalable diagnostic GFET devices based on the synergy between 2D semiconducting nanomaterials and affinity-based recognition elements.

■ ASSOCIATED CONTENT

Supporting Information

The Supporting Information is available free of charge at <https://pubs.acs.org/doi/10.1021/acsami.1c12142>.

Materials information, ellipsometric analysis, Raman spectroscopy details and peak assignments, in situ SPR PEGylation of PBSE surface curve, SPR curve for ConA binding and Mass surface density comparison, K_D calculation details, and clinically relevant concentration region of ferritin levels (PDF)

■ AUTHOR INFORMATION

Corresponding Authors

Esteban Piccinini – Instituto de Investigaciones Físicoquímicas Teóricas y Aplicadas (INIFTA), Departamento de Química, Facultad de Ciencias Exactas, Universidad Nacional de La

Plata, La Plata B1904DPI, Argentina;
Email: estebanpiccinini@inifta.unlp.edu.ar

Omar Azzaroni – Instituto de Investigaciones Físicoquímicas Teóricas y Aplicadas (INIFTA), Departamento de Química, Facultad de Ciencias Exactas, Universidad Nacional de La Plata, La Plata B1904DPI, Argentina; orcid.org/0000-0002-5098-0612; Email: azzaroni@inifta.unlp.edu.ar; <http://softmatter.quimica.unlp.edu.ar>

Authors

Juan A. Allegretto – Instituto de Investigaciones Físicoquímicas Teóricas y Aplicadas (INIFTA), Departamento de Química, Facultad de Ciencias Exactas, Universidad Nacional de La Plata, La Plata B1904DPI, Argentina; orcid.org/0000-0002-7371-2610

Juliana Scotto – Instituto de Investigaciones Físicoquímicas Teóricas y Aplicadas (INIFTA), Departamento de Química, Facultad de Ciencias Exactas, Universidad Nacional de La Plata, La Plata B1904DPI, Argentina

Agustín L. Cantillo – Instituto de Investigaciones Físicoquímicas Teóricas y Aplicadas (INIFTA), Departamento de Química, Facultad de Ciencias Exactas, Universidad Nacional de La Plata, La Plata B1904DPI, Argentina; GISENS BIOTECH, Ciudad Autónoma de Buenos Aires 1195, Argentina

Gonzalo E. Fenoy – Instituto de Investigaciones Físicoquímicas Teóricas y Aplicadas (INIFTA), Departamento de Química, Facultad de Ciencias Exactas, Universidad Nacional de La Plata, La Plata B1904DPI, Argentina; orcid.org/0000-0003-4336-4843

Waldemar A. Marmisollé – Instituto de Investigaciones Físicoquímicas Teóricas y Aplicadas (INIFTA), Departamento de Química, Facultad de Ciencias Exactas, Universidad Nacional de La Plata, La Plata B1904DPI, Argentina; orcid.org/0000-0003-0031-5371

Complete contact information is available at:
<https://pubs.acs.org/10.1021/acsami.1c12142>

Author Contributions

[§]E.P. and J.A.A. Joint first authors.

Notes

The authors declare the following competing financial interest(s): E.P., W.A.M. and O.A. are scientific advisors of GISENS BIOTECH through a cooperation agreement between UNLP, CONICET and GISENS Biotech. This statement is included in the manuscript.

ACKNOWLEDGMENTS

This work was supported by the following institutions: Universidad Nacional de La Plata (UNLP), ANPCYT (PICT 2018-04684, EBT COVID-19 No. 0017-IF-2020-85480721-APN-FONARSEC#ANPIDTYI), GISENS BIOTECH, and CONICET-UNLP-GISENS BIOTECH (700-2845/20-000). J.S., W.A.M., and O.A. are staff members of CONICET. J.A.A., G.E.F., and E.P. acknowledge their fellowship from CONICET.

REFERENCES

- (1) Zhang, H. Ultrathin Two-Dimensional Nanomaterials. *ACS Nano* **2015**, *9*, 9451–9469.
- (2) Tan, C.; Cao, X.; Wu, X.-J.; He, Q.; Yang, J.; Zhang, X.; Chen, J.; Zhao, W.; Han, S.; Nam, G.-H.; Sindoro, M.; Zhang, H. Recent

Advances in Ultrathin Two-Dimensional Nanomaterials. *Chem. Rev.* **2017**, *117*, 6225–6331.

- (3) Novoselov, K. S.; Geim, A. K.; Morozov, S. V.; Jiang, D.; Zhang, Y.; Dubonos, S. V.; Grigorieva, I. V.; Firsov, A. A. Electric Field in Atomically Thin Carbon Films. *Science* **2004**, *306*, 666–669.

- (4) Su, S.; Sun, Q.; Gu, X.; Xu, Y.; Shen, J.; Zhu, D.; Chao, J.; Fan, C.; Wang, L. Two-Dimensional Nanomaterials for Biosensing Applications. *TrAC, Trends Anal. Chem.* **2019**, *119*, No. 115610.

- (5) Zhang, X.; Jing, Q.; Ao, S.; Schneider, G. F.; Kireev, D.; Zhang, Z.; Fu, W. Ultrasensitive Field-Effect Biosensors Enabled by the Unique Electronic Properties of Graphene. *Small* **2020**, *16*, No. 1902820.

- (6) Fenoy, G. E.; Marmisollé, W. A.; Azzaroni, O.; Knoll, W. Acetylcholine Biosensor Based on the Electrochemical Functionalization of Graphene Field-Effect Transistors. *Biosens. Bioelectron.* **2020**, *148*, No. 111796.

- (7) Hess, L. H.; Lyuleeva, A.; Blaschke, B. M.; Sachsenhauser, M.; Seifert, M.; Garrido, J. A.; Deubel, F. Graphene Transistors with Multifunctional Polymer Brushes for Biosensing Applications. *ACS Appl. Mater. Interfaces* **2014**, *6*, 9705–9710.

- (8) Seo, G.; Lee, G.; Kim, M. J.; Baek, S. H.; Choi, M.; Ku, K. B.; Lee, C. S.; Jun, S.; Park, D.; Kim, H. G.; Kim, S.-J.; Lee, J.-O.; Kim, B. T.; Park, E. C.; Kim, S., II. Rapid Detection of COVID-19 Causative Virus (SARS-CoV-2) in Human Nasopharyngeal Swab Specimens Using Field-Effect Transistor-Based Biosensor. *ACS Nano* **2020**, *14*, 5135–5142.

- (9) Hajian, R.; Balderston, S.; Tran, T.; DeBoer, T.; Etienne, J.; Sandhu, M.; Wauford, N. A.; Chung, J. Y.; Nokes, J.; Athaiya, M.; Paredes, J.; Peytavi, R.; Goldsmith, B.; Murthy, N.; Conboy, I. M.; Aran, K. Detection of Unamplified Target Genes via CRISPR–Cas9 Immobilized on a Graphene Field-Effect Transistor. *Nat. Biomed. Eng.* **2019**, *3*, 427–437.

- (10) Morales-Narváez, E.; Dincer, C. The Impact of Biosensing in a Pandemic Outbreak: COVID-19. *Biosens. Bioelectron.* **2020**, *163*, No. 112274.

- (11) Yakoh, A.; Pimpitak, U.; Rengpipat, S.; Hirankarn, N.; Chailapakul, O.; Chaiyo, S. Paper-Based Electrochemical Biosensor for Diagnosing COVID-19: Detection of SARS-CoV-2 Antibodies and Antigen. *Biosens. Bioelectron.* **2021**, *176*, No. 112912.

- (12) Alafeef, M.; Dighe, K.; Moitra, P.; Pan, D. Rapid, Ultrasensitive, and Quantitative Detection of SARS-CoV-2 Using Antisense Oligonucleotides Directed Electrochemical Biosensor Chip. *ACS Nano* **2020**, *14*, 17028–17045.

- (13) Liu, J.; Liu, Z.; Barrow, C. J.; Yang, W. Molecularly Engineered Graphene Surfaces for Sensing Applications: A Review. *Anal. Chim. Acta* **2015**, *859*, 1–19.

- (14) Niyogi, S.; Bekyarova, E.; Itkis, M. E.; Zhang, H.; Shepperd, K.; Hicks, J.; Sprinkle, M.; Berger, C.; Lau, C. N.; deHeer, W. A.; Conrad, E. H.; Haddon, R. C. Spectroscopy of Covalently Functionalized Graphene. *Nano Lett.* **2010**, *10*, 4061–4066.

- (15) Ramasubramaniam, A.; Selhorst, R.; Alon, H.; Barnes, M. D.; Emrick, T.; Naveh, D. Combining 2D Inorganic Semiconductors and Organic Polymers at the Frontier of the Hard-Soft Materials Interface. *J. Mater. Chem. C* **2017**, *5*, 11158–11164.

- (16) Nandanapalli, K. R.; Mudusu, D.; Lee, S. Functionalization of Graphene Layers and Advancements in Device Applications. In *Carbon*; Elsevier Ltd., November 1, 2019; *152*, pp 954–985.

- (17) Loh, K. P.; Bao, Q.; Ang, P. K.; Yang, J. The Chemistry of Graphene. *J. Mater. Chem.* **2010**, *20*, 2277.

- (18) Andoy, N. M.; Filipiak, M. S.; Vetter, D.; Gutiérrez-Sanz, Ó.; Tarasov, A. Graphene-Based Electronic Immunosensor with Femtomolar Detection Limit in Whole Serum. *Adv. Mater. Technol.* **2018**, *3*, No. 1800186.

- (19) Hao, Z.; Zhu, Y.; Wang, X.; Rotti, P. G.; Dimarco, C.; Tyler, S. R.; Zhao, X.; Engelhardt, J. F.; Hone, J.; Lin, Q. Real-Time Monitoring of Insulin Using a Graphene Field-Effect Transistor Aptameric Nanosensor. *ACS Appl. Mater. Interfaces* **2017**, *9*, 27504–27511.

- (20) Kohmoto, M.; Ozawa, H.; Yang, L.; Hagio, T.; Matsunaga, M.; Haga, M. A. Controlling the Adsorption of Ruthenium Complexes on Carbon Surfaces through Noncovalent Bonding with Pyrene Anchors: An Electrochemical Study. *Langmuir* **2016**, *32*, 4141–4152.
- (21) Cao, M.; Fu, A.; Wang, Z.; Liu, J.; Kong, N.; Zong, X.; Liu, H.; Gooding, J. J. Electrochemical and Theoretical Study of π - π Stacking Interactions between Graphitic Surfaces and Pyrene Derivatives. *J. Phys. Chem. C* **2014**, *118*, 2650–2659.
- (22) Mann, J. A.; Rodríguez-López, J.; Abruña, H. D.; Dichtel, W. R. Multivalent Binding Motifs for the Noncovalent Functionalization of Graphene. *J. Am. Chem. Soc.* **2011**, *133*, 17614–17617.
- (23) Cheng, N.; Brown, A. A.; Azzaroni, O.; Huck, W. T. S. Thickness-Dependent Properties of Polyzwitterionic Brushes. *Macromolecules* **2008**, *41*, 6317–6321.
- (24) Mir, M.; Cameron, P. J.; Zhong, X.; Azzaroni, O.; Álvarez, M.; Knoll, W. Anti-Fouling Characteristics of Surface-Confined Oligonucleotide Strands Bioconjugated on Streptavidin Platforms in the Presence of Nanomaterials. *Talanta* **2009**, *78*, 1102–1106.
- (25) Mann, J. A.; Alava, T.; Craighead, H. G.; Dichtel, W. R. Preservation of Antibody Selectivity on Graphene by Conjugation to a Tripod Monolayer. *Angew. Chem.* **2013**, *125*, 3259–3262.
- (26) Gao, N.; Gao, T.; Yang, X.; Dai, X.; Zhou, W.; Zhang, A.; Lieber, C. M. Specific Detection of Biomolecules in Physiological Solutions Using Graphene Transistor Biosensors. *Proc. Natl. Acad. Sci. U.S.A.* **2016**, *113*, 14633–14638.
- (27) Gao, N.; Zhou, W.; Jiang, X.; Hong, G.; Fu, T. M.; Lieber, C. M. General Strategy for Biodection in High Ionic Strength Solutions Using Transistor-Based Nanoelectronic Sensors. *Nano Lett.* **2015**, *15*, 2143–2148.
- (28) Piccinini, E.; Alberti, S.; Longo, G. S.; Berninger, T.; Brey, J.; Dostalek, J.; Azzaroni, O.; Knoll, W. Pushing the Boundaries of Interfacial Sensitivity in Graphene FET Sensors: Polyelectrolyte Multilayers Strongly Increase the Debye Screening Length. *J. Phys. Chem. C* **2018**, *122*, 10181–10188.
- (29) Aspermaier, P.; Ramach, U.; Reiner-Rozman, C.; Fossati, S.; Lechner, B.; Moya, S. E.; Azzaroni, O.; Dostalek, J.; Szunerits, S.; Knoll, W.; Binting, J. Dual Monitoring of Surface Reactions in Real Time by Combined Surface-Plasmon Resonance and Field-Effect Transistor Interrogation. *J. Am. Chem. Soc.* **2020**, *142*, 11709–11716.
- (30) Berninger, T.; Bliem, C.; Piccinini, E.; Azzaroni, O.; Knoll, W. Cascading Reaction of Arginase and Urease on a Graphene-Based FET for Ultrasensitive, Real-Time Detection of Arginine. *Biosens. Bioelectron.* **2018**, *115*, 104–110.
- (31) Piccinini, E.; Bliem, C.; Reiner-Rozman, C.; Battaglini, F.; Azzaroni, O.; Knoll, W. Enzyme-Polyelectrolyte Multilayer Assemblies on Reduced Graphene Oxide Field-Effect Transistors for Biosensing Applications. *Biosens. Bioelectron.* **2017**, *92*, 661–667.
- (32) Morales-Sanfrutos, J.; Lopez-Jaramillo, J.; Ortega-Muñoz, M.; Megia-Fernandez, A.; Perez-Balderas, F.; Hernandez-Mateo, F.; Santoyo-Gonzalez, F. Vinyl Sulfone: A Versatile Function for Simple Bioconjugation and Immobilization. *Org. Biomol. Chem.* **2010**, *8*, 667–675.
- (33) Lin, G. G. H.; Scott, J. G. Investigations of the Constitutive Overexpression of CYP6D1 in the Permethrin Resistant LPR Strain of House Fly (*Musca Domestica*). *Pestic. Biochem. Physiol.* **2011**, *100*, 130–134.
- (34) Hermanson, G. T. The Reactions of Bioconjugation. In *Bioconjugate Techniques*; Elsevier, 2013; pp 229–258.
- (35) Dos Santos, J. C. S.; Rueda, N.; Barbosa, O.; Fernández-Sánchez, J. F.; Medina-Castillo, A. L.; Ramón-Márquez, T.; Arias-Martos, M. C.; Millán-Linares, M. C.; Pedroche, J.; Yust, M. D. M.; Gonçalves, L. R. B.; Fernandez-Lafuente, R. Characterization of Supports Activated with Divinyl Sulfone as a Tool to Immobilize and Stabilize Enzymes via Multipoint Covalent Attachment. Application to Chymotrypsin. *RSC Adv.* **2015**, *5*, 20639–20649.
- (36) Bliem, C.; Piccinini, E.; Knoll, W.; Azzaroni, O. Enzyme Multilayers on Graphene-Based FETs for Biosensing Applications. In *Methods in Enzymology*; Academic Press Inc., 2018; Vol. 609, pp 23–46.
- (37) Sappia, L. D.; Piccinini, E.; Marmisollé, W.; Santilli, N.; Maza, E.; Moya, S.; Battaglini, F.; Madrid, R. E.; Azzaroni, O. Integration of Biorecognition Elements on PEDOT Platforms through Supramolecular Interactions. *Adv. Mater. Interfaces* **2017**, *4*, No. 1700502.
- (38) Kolańska, M.; Krastev, R.; Warszyński, P. Characteristics of Polyelectrolyte Multilayers: Effect of PEI Anchoring Layer and Posttreatment after Deposition. *J. Colloid Interface Sci.* **2007**, *305*, 46–56.
- (39) Wang, H.; Cheng, F.; Li, M.; Peng, W.; Qu, J. Reactivity and Kinetics of Vinyl Sulfone-Functionalized Self-Assembled Monolayers for Bioactive Ligand Immobilization. *Langmuir* **2015**, *31*, 3413–3421.
- (40) Sappia, L. D.; Piccinini, E.; von Binderling, C.; Knoll, W.; Marmisollé, W.; Azzaroni, O. PEDOT-Polyamine Composite Films for Bioelectrochemical Platforms - Flexible and Easy to Derivatize. *Mater. Sci. Eng. C* **2020**, *109*, No. 110575.
- (41) Cheng, F.; Shang, J.; Ratner, D. M. A Versatile Method for Functionalizing Surfaces with Bioactive Glycans. *Bioconjug. Chem.* **2011**, *22*, 50–57.
- (42) Patterson, J. T.; Asano, S.; Li, X.; Rader, C.; Barbas, C. F. Improving the Serum Stability of Site-Specific Antibody Conjugates with Sulfone Linkers. *Bioconjug. Chem.* **2014**, *25*, 1402–1407.
- (43) Li, M.; Cheng, F.; Li, H.; Jin, W.; Chen, C.; He, W.; Cheng, G.; Wang, Q. Site-Specific and Covalent Immobilization of His-Tagged Proteins via Surface Vinyl Sulfone-Imidazole Coupling. *Langmuir* **2019**, *35*, 16466–16475.
- (44) Banerjee, I.; Pangule, R. C.; Kane, R. S. Antifouling Coatings: Recent Developments in the Design of Surfaces That Prevent Fouling by Proteins, Bacteria, and Marine Organisms. *Adv. Mater.* **2011**, *23*, 690–718.
- (45) Hao, Z.; Pan, Y.; Huang, C.; Wang, Z.; Lin, Q.; Zhao, X.; Liu, S. Modulating the Linker Immobilization Density on Aptameric Graphene Field Effect Transistors Using an Electric Field. *ACS Sensors* **2020**, *5*, 2503–2513.
- (46) Agrawal, B. B. L.; Goldstein, I. J. Protein-Carbohydrate Interaction. VII. Physical and Chemical Studies on Concanavalin A, the Hemagglutinin of the Jack Bean. *Arch. Biochem. Biophys.* **1968**, *124*, 218–229.
- (47) Pallarola, D.; Von Biderling, C.; Pietrasanta, L. I.; Queralto, N.; Knoll, W.; Battaglini, F.; Azzaroni, O. Recognition-Driven Layer-by-Layer Construction of Multiprotein Assemblies on Surfaces: A Biomolecular Toolkit for Building up Chemosensitive Bioelectrochemical Interfaces. *Phys. Chem. Chem. Phys.* **2012**, *14*, 11027–11039.
- (48) Piccinini, E.; Pallarola, D.; Battaglini, F.; Azzaroni, O. Recognition-Driven Assembly of Self-Limiting Supramolecular Protein Nanoparticles Displaying Enzymatic Activity. *Chem. Commun.* **2015**, *51*, 14754–14757.
- (49) Pallarola, D.; Queralto, N.; Battaglini, F.; Azzaroni, O. Supramolecular Assembly of Glucose Oxidase on Concanavalin A-Modified Gold Electrodes. *Phys. Chem. Chem. Phys.* **2010**, *12*, 8071–8083.
- (50) Pallarola, D.; Queralto, N.; Knoll, W.; Azzaroni, O.; Battaglini, F. Facile Glycoenzyme Wiring to Electrode Supports by Redox-Active Biosupramolecular Glue. *Chem. - A Eur. J.* **2010**, *16*, 13970–13975.
- (51) Pallarola, D.; Queralto, N.; Knoll, W.; Ceoli, A.; Azzaroni, O.; Battaglini, F. Redox-Active Concanavalin A: Synthesis, Characterization, and Recognition-Driven Assembly of Interfacial Architectures for Bioelectronic Applications. *Langmuir* **2010**, *26*, 13684–13696.
- (52) Chung, K.; Rani, A.; Lee, J. E.; Kim, J. E.; Kim, Y.; Yang, H.; Kim, S. O.; Kim, D.; Kim, D. H. Systematic Study on the Sensitivity Enhancement in Graphene Plasmonic Sensors Based on Layer-by-Layer Self-Assembled Graphene Oxide Multilayers and Their Reduced Analogues. *ACS Appl. Mater. Interfaces* **2015**, *7*, 144–151.
- (53) Subramanian, P.; Lesniewski, A.; Kaminska, I.; Vlandas, A.; Vasilescu, A.; Niedziolka-Jonsson, J.; Pichonat, E.; Happy, H.; Boukherroub, R.; Szunerits, S. Lysozyme Detection on Aptamer Functionalized Graphene-Coated SPR Interfaces. *Biosens. Bioelectron.* **2013**, *50*, 239–243.

(54) Tao, C.; Zhang, J.; Yang, S. Preparation and Biocompatibility of BSA Monolayer on Silicon Surface. *J. Nanosci. Nanotechnol.* **2011**, *11*, 5068–5074.

(55) Cortez, M. L.; Pallarola, D.; Ceolín, M.; Azzaroni, O.; Battaglini, F. Electron Transfer Properties of Dual Self-Assembled Architectures Based on Specific Recognition and Electrostatic Driving Forces: Its Application to Control Substrate Inhibition in Horseradish Peroxidase-Based Sensors. *Anal. Chem.* **2013**, *85*, 2414–2422.

(56) Katrlík, J.; Škrabana, R.; Mislovičová, D.; Gemeiner, P. Binding of D-Mannose-Containing Glycoproteins to d-Mannose-Specific Lectins Studied by Surface Plasmon Resonance. *Colloids Surf., A* **2011**, *382*, 198–202.

(57) Mislovičová, D.; Katrlík, J.; Paulovičová, E.; Gemeiner, P.; Tkáč, J. Comparison of Three Distinct ELLA Protocols for Determination of Apparent Affinity Constants between Con A and Glycoproteins. *Colloids Surf., B* **2012**, *94*, 163–169.

(58) Fabiani, L.; Saroglia, M.; Galatà, G.; De Santis, R.; Fillo, S.; Luca, V.; Faggioni, G.; D'Amore, N.; Regalbuto, E.; Salvatori, P.; Terova, G.; Moscone, D.; Lista, F.; Arduini, F. Magnetic Beads Combined with Carbon Black-Based Screen-Printed Electrodes for COVID-19: A Reliable and Miniaturized Electrochemical Immunosensor for SARS-CoV-2 Detection in Saliva. *Biosens. Bioelectron.* **2021**, *171*, No. 112686.

(59) Wang, J.; Jiang, M.; Chen, X.; Montaner, L. J. Cytokine Storm and Leukocyte Changes in Mild versus Severe SARS-CoV-2 Infection: Review of 3939 COVID-19 Patients in China and Emerging Pathogenesis and Therapy Concepts. In *Journal of Leukocyte Biology*; John Wiley and Sons Inc., July 1, 2020; pp 17–41.

(60) Zhou, F.; Yu, T.; Du, R.; Fan, G.; Liu, Y.; Liu, Z.; Xiang, J.; Wang, Y.; Song, B.; Gu, X.; Guan, L.; Wei, Y.; Li, H.; Wu, X.; Xu, J.; Tu, S.; Zhang, Y.; Chen, H.; Cao, B. Clinical Course and Risk Factors for Mortality of Adult Inpatients with COVID-19 in Wuhan, China: A Retrospective Cohort Study. *Lancet* **2020**, *395*, 1054–1062.

(61) Wang, Q.; Zhang, Y.; Wu, L.; Niu, S.; Song, C.; Zhang, Z.; Lu, G.; Qiao, C.; Hu, Y.; Yuen, K. Y.; Wang, Q.; Zhou, H.; Yan, J.; Qi, J. Structural and Functional Basis of SARS-CoV-2 Entry by Using Human ACE2. *Cell* **2020**, *181*, 894–904.e9.

(62) Wrapp, D.; Wang, N.; Corbett, K. S.; Goldsmith, J. A.; Hsieh, C.-L.; Abiona, O.; Graham, B. S.; McLellan, J. S. Cryo-EM Structure of the 2019-NCoV Spike in the Prefusion Conformation. *Science* **2020**, *367*, 1260–1263.

(63) Walls, A. C.; Park, Y.-J.; Tortorici, M. A.; Wall, A.; McGuire, A. T.; Velesler, D. Structure, Function, and Antigenicity of the SARS-CoV-2 Spike Glycoprotein. *Cell* **2020**, *181*, 281–292.e6.

(64) Lan, J.; Ge, J.; Yu, J.; Shan, S.; Zhou, H.; Fan, S.; Zhang, Q.; Shi, X.; Wang, Q.; Zhang, L.; Wang, X. Structure of the SARS-CoV-2 Spike Receptor-Binding Domain Bound to the ACE2 Receptor. *Nature* **2020**, *581*, 215–220.

(65) Kim, H. Y.; Lee, J. H.; Kim, M. J.; Park, S. C.; Choi, M.; Lee, W.; Ku, K. B.; Kim, B. T.; Changkyun Park, E.; Kim, H. G.; Kim, S., II Development of a SARS-CoV-2-Specific Biosensor for Antigen Detection Using ScFv-Fc Fusion Proteins. *Biosens. Bioelectron.* **2021**, *175*, No. 112868.

(66) Bonam, S. R.; Kaveri, S. V.; Sakuntabhai, A.; Gilardin, L.; Bayry, J. Adjunct Immunotherapies for the Management of Severely Ill COVID-19 Patients. *Cell Rep. Med.* **2020**, *1*, No. 100016.